The Astrophysical Journal, 572:L39–L43, 2002 June 10
© 2002. The American Astronomical Society. All rights reserved. Printed in U.S.A.

COLLAPSE OF A ROTATING SUPERMASSIVE STAR TO A SUPERMASSIVE BLACK HOLE: FULLY RELATIVISTIC SIMULATIONS

Masaru Shibata[1] and Stuart L. Shapiro[2,3]
Received 2001 December 28; accepted 2002 May 1; published 2002 May 20

ABSTRACT

We follow the collapse in axisymmetry of a uniformly rotating, supermassive star (SMS) to a supermassive black hole in full general relativity. The initial SMS of arbitrary mass M is marginally unstable to radial collapse and rotates at the mass-shedding limit. The collapse proceeds homologously early on and results in the appearance of an apparent horizon at the center. Although our integration terminates before final equilibrium is achieved, we determine that the final black hole will contain about 90% of the total mass of the system and will have a spin parameter $J/M^2 \sim 0.75$. The remaining gas forms a rotating disk about the nascent hole.

Subject headings: black hole physics — hydrodynamics — relativity — stars: rotation

1. INTRODUCTION

Recent observations provide increasingly strong evidence that supermassive black holes (SMBHs) of mass $\sim 10^6$–$10^{10}\,M_\odot$ exist and that they are the central engines that power active galactic nuclei and quasars (Rees 1998, 2001). The dynamical formation of SMBHs as well as the in-spiral, collision, and merger of binary SMBHs are promising sources of long-wavelength gravitational waves for the proposed Laser Interferometer Space Antenna (Thorne 1995; Schutz 2001). However, the actual scenario(s) by which SMBHs form is (are) still uncertain. Viable stellar dynamical and hydrodynamical routes leading to the formation of SMBHs have been proposed (e.g., Begelman & Rees 1978; Rees 1984, 1998, 2001; Shapiro & Teukolsky 1985; Quinlan & Shapiro 1990; Balberg & Shapiro 2002). In typical hydrodynamical scenarios, a supermassive gas cloud is built up from the multiple collisions of stars or small gas clouds in stellar clusters to form a supermassive star (SMS; Begelman & Rees 1978). A supermassive gas cloud might be formed from scattered gas in the bulge that falls into the central region because of radiation drag (Umemura 2001). SMSs ultimately collapse to black holes following quasi-stationary cooling and contraction to the onset of radial instability (Zel'dovich & Novikov 1971; Shapiro & Teukolsky 1983). This scenario for forming a SMBH following SMS collapse was investigated in the 1960s and 1970s, but the studies either treated nonrotating configurations and assumed spherical symmetry or employed approximate analytical models (see, e.g., Baumgarte & Shapiro 1999 for a review and references).

However, SMSs are likely to be rapidly rotating (see, e.g., Loeb & Rasio 1994). Baumgarte & Shapiro (1999) recently performed a detailed numerical analysis of the structure and stability of a rapidly rotating SMS in equilibrium. Assuming that the viscous or magnetic braking timescale for angular momentum transfer is shorter than the evolution timescale of a typical SMS (Zel'dovich & Novikov 1971; see New & Shapiro 2001 for an alternative), the star will settle into rigid rotation and evolve to the mass-shedding limit following cooling and contraction. (At the mass-shedding limit, the angular velocity of gas at the equator equals the Kepler velocity.) They found that all stars at the onset of quasi-radial collapse have an equatorial radius $R \approx 640GM/c^2$ and a nondimensional spin parameter $q \equiv cJ/GM^2 \approx 0.97$. Here J, M, c, and G are the spin, gravitational mass, light velocity, and gravitational constant, respectively. (Hereafter, we adopt gravitational units and set $c = G = 1$.) Because of the large value of q, it is uncertain whether the rotating SMS collapses directly to a black hole or forms a disk. Saijo et al. (2002) investigated the collapse of a rotating SMS in a post-Newtonian (PN) approximation and concluded that the effects of rotation do not halt the collapse and that a SMBH is likely to be formed. However, a PN calculation cannot follow collapse into the strong-field regime and cannot rigorously address the possibility of black hole formation and growth, or the final outcome.

To clarify whether a SMBH forms as the endpoint of rapidly rotating SMS collapse and, if it does, to determine the final hole parameters, we performed a fully general relativistic numerical simulation of the collapse in axisymmetry. We demonstrate that the collapse indeed leads directly to a SMBH of moderately rapid rotation, with $q \sim 0.75$.

2. COMPUTATIONAL SETUP

Simulations were performed using an axisymmetric code in full general relativity (Shibata 2000). This code was constructed from a three-dimensional code (Shibata 1999b) using the so-called cartoon method in numerical relativity (Alcubierre et al. 2001): we solve the Einstein field equations in Cartesian coordinates with a grid of size $(N, 3, N)$ in (x, y, z), covering a computational domain of $0 \le x, z \le L$, and $-\Delta y \le y \le \Delta y$. Here N is a constant ($\gg 1$), L is the location of the outer boundary, and Δy is the grid spacing in the y-direction, with an axisymmetric boundary condition imposed at $y = \pm\Delta y$; the spin axis is along z. We solve the hydrodynamic equations with an axisymmetric code in cylindrical coordinates. This hydrodynamical code was calibrated by numerous test calculations, including the spherical collapse of dust, the stability of spherical stars, mode analysis of spherical stars, and the evolution of rotating stars (Shibata 1999b). We adopt maximal time slicing and approximate minimal distortion as coordinate gauge conditions throughout the simulation (Shibata 1999a, 1999b). Formation of a black hole is determined by finding an apparent horizon.

Violations of the Hamiltonian constraint and the conservation of mass and angular momentum are monitored as a numerical accuracy check during the simulation. The total angular

[1] Graduate School of Arts and Sciences, University of Tokyo, Komaba, Meguro, Tokyo 153-8902, Japan.
[2] Department of Physics, University of Illinois at Urbana-Champaign, 1110 West Green Street, Urbana, IL 61801-3080.
[3] Department of Astronomy and National Center for Supercomputing Applications, University of Illinois at Urbana-Champaign, 1002 West Green Street, Urbana, IL 61801-3080.

momentum J and total baryon rest mass M_* should be strictly conserved in axisymmetry. The gravitational mass M is not conserved, because of the emission of gravitational radiation, but the decrease in M is very small.

Since the SMS spins up during the collapse, a nonaxisymmetric instability could arise. However, the PN study by Saijo et al. (2002) indicates that such an instability is not excited, at least when the equatorial radius of the collapsing star exceeds $10M$. By restricting our analysis to axisymmetry, we can improve our resolution by a factor of $\gtrsim 10$ of the strong-field central region where the black hole forms.

To model the initial equilibrium SMS, we adopt a polytropic equation of state with the adiabatic index $\Gamma = 4/3$, setting $P = K\rho^{4/3}$, where P and ρ are the pressure and rest mass density, respectively. This prescription is appropriate for a radiation-dominated SMS equation of state. Here K is a constant whose value determines the mass; we scale out the mass by setting $K = 1$ (Baumgarte & Shapiro 1999).

Although a spherical SMS with the adopted equation of state is unconditionally unstable to collapse, rotation can stabilize the star. We focus only on a rigidly rotating SMS at the mass-shedding limit. According to Baumgarte & Shapiro (1999), rotating SMSs with equatorial radii $R < 640M$ are unstable against collapse. At $R \approx 640M$, the ratio of the rotational kinetic energy to the gravitational binding energy T/W is about 0.009, and $q \approx 0.97$.

We chose a SMS with $R \approx 620M$, a star that is located just beyond the critical point of instability. In this case, we have $T/W \approx 0.0088$ and $q \approx 0.96$, values that are nearly equal to those of the critical configuration (see Table 1). A second simulation was performed for a more compact star with $R \approx 570M$, but our results were essentially unchanged. To accelerate the collapse, we depleted the pressure by 1% initially. During the evolution, we adopted a Γ-law equation of state according to $P = (\Gamma - 1)\rho\epsilon$, where ϵ denotes the specific internal energy of the fluid, thereby treating the gas as an ideal, adiabatic fluid in which cooling can be ignored on a dynamical timescale (Linke et al. 2001).

Since the equatorial radius decreases by a factor of ~ 1000 (from $\sim 600M$ to $\lesssim M$), using a fixed uniform grid with sufficient resolution for all epochs would be computationally prohibitive. Instead, we adopted a uniform grid with decreasing grid spacing and increasing grid number as the collapse proceeded, in order to guarantee adequate resolution up to the formation of an apparent horizon. For the early stages, where the radius at the equatorial surface R_m exceeds $150M$, we used $N = 300$ grid points in the x- and z-directions. Here we identify R_m as the radius at which $\rho = 10^{-6}\rho_{\max}$, where $\rho_{\max}$ is the maximum interior density. Initially, the grid covers the equator with about 200 grid points. The outer boundaries along the x- and z-axes are located at $L \approx 930M$.

Since T/W is small and $\Gamma = 4/3$, the collapse proceeds in a homologous manner in the central regions during the early stages (Shapiro & Teukolsky 1979; Goldreich & Weber 1980; Saijo et al. 2002). Taking advantage of this behavior, we rezoned by moving the outer boundary inward and decreasing the grid spacing, keeping $N(=300)$ fixed. All quantities in the new grid are calculated using cubic interpolation. We discarded the outermost computational domain, but the discarded baryon rest mass is very small (less than 10^{-4} of the total) when $R_m \gtrsim 150M$. We repeated this procedure twice until homology breaks down at $R_m \lesssim 150M$. After this stage, the collapse timescale in the central region is much shorter than in the envelope. Consequently, we increased the grid number N and decreased Δ, monitoring the lapse function at the center α_0. Specifically, we set N and L as follows: for $\alpha_0 \geq 0.90$, we set $N = 600$ and $L \approx 233M$; for $0.70 \leq \alpha_0 \leq 0.90$, we set $N = 900$ and $L \approx 155M$; and for $0.30 \leq \alpha_0 \leq 0.70$, we set $N = 1200$ and $L \approx 116M$. With this treatment, the discarded fraction of the baryon rest mass is only $\sim 0.15\%$ down to $\alpha_0 = 0.3$.

TABLE 1
PARAMETERS OF THE INITIAL SMS

Parameter	Initial Data
Radius at equator R/M	622
T/W[a]	0.0088
q	0.96
Gravitational mass M	4.566
Baryon rest mass M_*	4.566
Angular velocity Ω	1.40E−5
Central density ρ_c	7.84E−9

NOTE.—All the quantities are shown in units of $c = G = K = 1$.

[a] Ratio of the kinetic energy to the gravitational binding energy.

For $\alpha_0 \lesssim 0.3$, the central density profile becomes very steep. To see its dependence on the grid resolution during black hole formation, we carried out simulations using different combinations of N and L to refine the grid, with the restriction that $N \leq 2400$. The setup of each simulation was as follows: (A) for $\alpha_0 \leq 0.30$, we took $N = 1200$ and $L \approx 116M$, with no regridding at $\alpha_0 = 0.3$; (B) for $\alpha_0 \leq 0.30$, we took $N = 1200$ and $L \approx 58M$, regridding once at $\alpha_0 = 0.3$; (C) for $0.05 \leq \alpha_0 \leq 0.30$, we took $N = 1200$ and $L \approx 58M$, and for $\alpha_0 \leq 0.05$, we took $N = 1200$ and $L \approx 29M$; and (D) for $0.05 \leq \alpha_0 \leq 0.30$, we took $N = 1200$ and $L \approx 58M$, and for $\alpha_0 \leq 0.05$, we took $N = 2400$ and $L \approx 58M$. For cases C and D, we carried out regridding at $\alpha_0 = 0.3$ and 0.05. The minimum grid spacings for cases A–D were $0.097M$, $0.048M$, $0.024M$, and $0.024M$, respectively. The results for case D are the most reliable, but the results for the four cases do not differ significantly.

For cases B–D, the outer boundaries reside deep inside the stellar surface. Hence, the fluid at a large equatorial radius is discarded. When we allow $L \approx 58M$ ($29M$), the loss of the total baryon rest mass becomes $\sim 2\%$ (4%). Since the outer envelope has larger specific angular momentum, setting $L \approx 58M$ ($29M$) implies that $\sim 8\%$ (18%) of the total angular momentum is lost. As shown below, however, discarding some mass in the outer region has a tiny effect on the formation and evolution of a SMBH in the central region.

3. NUMERICAL RESULTS

In Figure 1, we display snapshots of density contours and velocity vectors in the x-z plane at selected times. Here the velocity field is defined as u^i/u^t, where u^μ is the four-velocity. The collapse proceeds nearly homologously in the central region during the early stages. However, for $R_m \lesssim 150M$, the effects of rotation and general relativity modify this property, when the collapse near the central region accelerates significantly.

In Figure 2, we show the time evolution of the central conformal factor ($\psi_0 \equiv [\det(\gamma_{ij})]^{1/12}$ at $r = 0$, where γ_{ij} denotes the three-dimensional spatial metric) and α_0 for cases A–D. We find that the collapse proceeds in a runaway manner in the final stages, although the time development depends somewhat on our adopted choice of time slicing.

Since $\psi^2\Delta$ measures the proper physical length of the grid spacing, maintaining the resolution requires changing Δ as $\Delta \propto \psi^{-2}$ (i.e., $N \propto \psi^2$). However, ψ diverges very sharply at

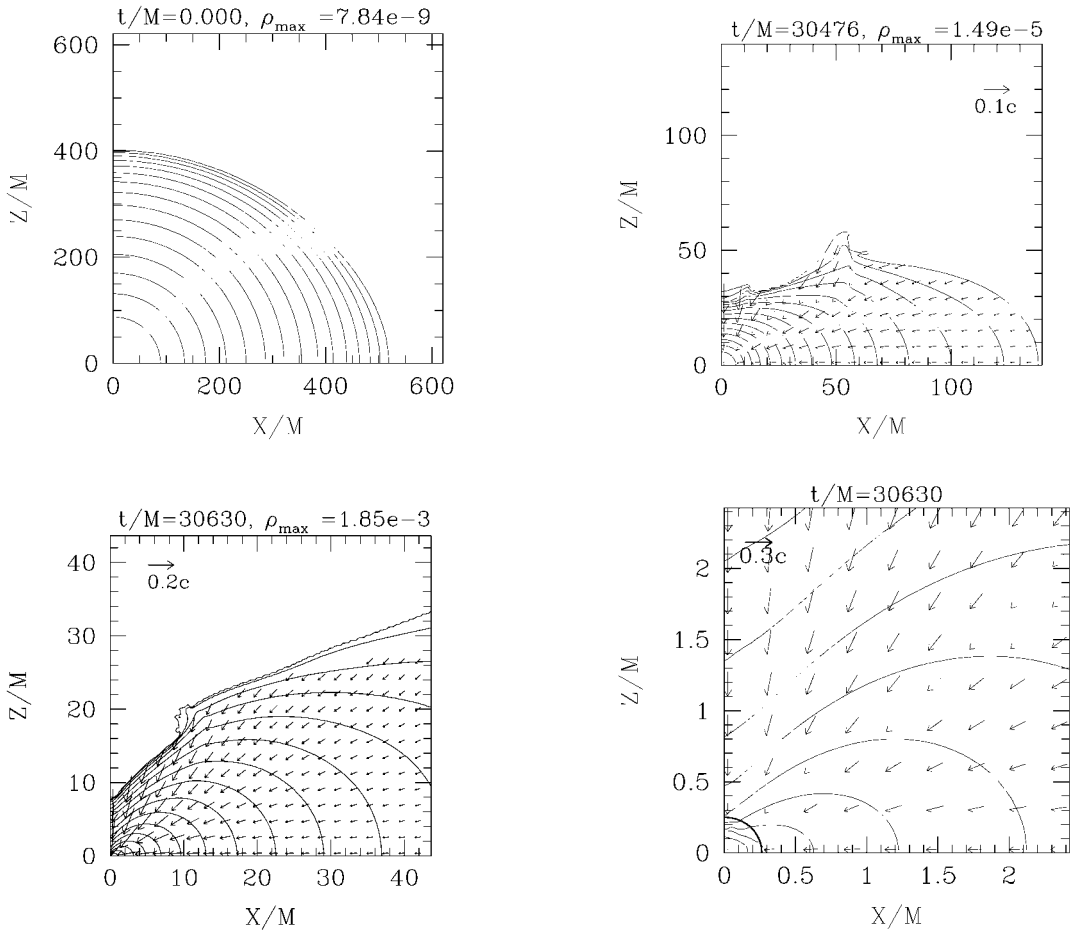

FIG. 1.—Snapshots of density contours and velocity vectors in the x-z plane at selected times for case D. The contours are drawn for $\rho/\rho_{\max} = 10^{-0.4j}$ ($j = 0 \sim 15$), where $\rho_{\max}$ denotes the maximum density at each time. The fourth rightmost panel is a blowup of the third panel in the central region; the thick solid curve at $r \approx 0.3M$ shows the location of the apparent horizon.

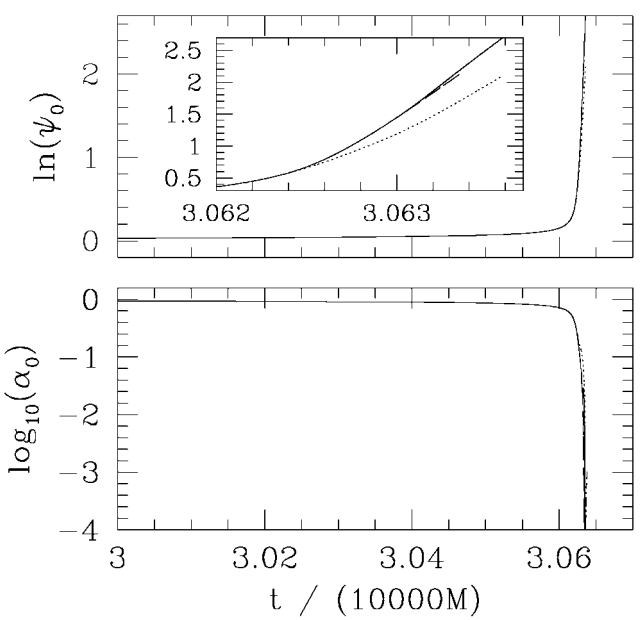

FIG. 2.—Central value of the conformal factor ψ_0 and lapse function α_0 as a function of time. The solid, dotted, dashed, and dot-dashed curves denote the results for cases D, A, B, and C. The results for cases C and D are not distinguishable.

late times, so increasing N by a factor of a few does not improve the resolution much. Accordingly, we terminated the simulation when the conservation of M was violated by ~10% at $t/M \approx 30636$.

There are two reasons for this runaway behavior at the center. One is that the equation of state is very soft, which produces stars with very centrally condensed structures. The collapse timescale in the central region is then much shorter than that in the outer region. The other reason is our choice of a coordinate (shift) condition, for which the resolution near the center deteriorates ("grid sucking"; see Shibata 1999b). Integrating to a final equilibrium state evidently requires different time and/or spatial gauge conditions.

We find an apparent horizon forms for $t/M \gtrsim 30630$. In Figure 3, we show the mass of the apparent horizon as a function of time. The mass is defined as $M_{\rm AH} \equiv (A/16\pi)^{1/2}$, where A denotes the area of the apparent horizon (e.g., Cook & York 1990). In addition to $M_{\rm AH}$, we plot the total baryon rest mass inside the apparent horizon $M_{*,\rm AH}$ for case D (*dotted curve*), which agrees approximately with $M_{\rm AH}$. Figure 3 illustrates that at the end of the simulation, about 60% of the total rest mass already has been swallowed into the black hole. Clearly, *collapse of a rapidly and uniformly rotating SMS leads to formation of a SMBH*. However, our final snapshot is not the final state because $M_{\rm AH}$ is still increasing.

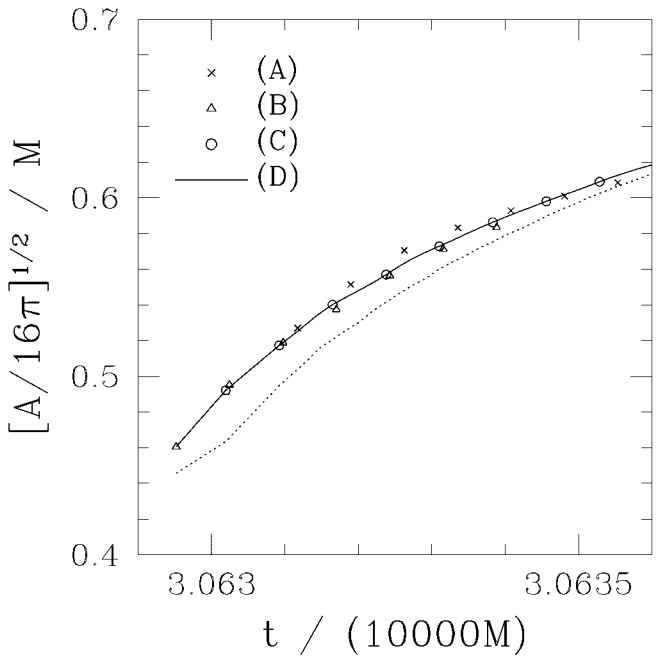

FIG. 3.—Evolution of the mass of apparent horizon (*solid curve*) and baryon rest mass inside the apparent horizon ($M_{*,\mathrm{AH}}$, *dotted curve*) as a function of time for case D. Mass and time are shown in units of the total gravitational mass M. For comparison, we also plot the mass of the apparent horizon as a function of time for cases A (*crosses*), B (*triangles*), and C (*circles*). The results for cases B, C, and D essentially agree.

It is possible to estimate what the final mass and spin of the black hole will be once it settles into equilibrium. Let us define the specific angular momentum according to $j \equiv hu_\varphi$, where $h(= 1 + \epsilon + P/\rho)$ is the specific enthalpy. In an axisymmetric system, the integrated baryon rest mass of all fluid elements with j less than a given value j_0, $m_*(j_0)$ (the angular momentum spectrum), is conserved in the absence of viscosity (Stark & Piran 1987):

$$m_*(j_0) = \int_{j<j_0} \rho\alpha u^t \psi^6 \, d^3x. \tag{1}$$

Let us consider the innermost stable circular orbit (ISCO) around the growing black hole at the center. If j of a fluid element is less than the value at the ISCO (j_{ISCO}), the element will fall into the black hole eventually. Now the possibility exists that some fluid can be captured even for $j > j_{\mathrm{ISCO}}$, if it is in a noncircular orbit. Ignoring these trajectories yields the minimum amount of mass that will fall into the black hole at each moment. The value of j_{ISCO} changes as the black hole grows. If j_{ISCO} increases, additional mass will fall into the black hole. However, if j_{ISCO} decreases, ambient fluid will no longer be captured. This expectation implies that when j_{ISCO} reaches a maximum value, the dynamical growth of the black hole will terminate.

To analyze the growth of the black hole mass, we generated Figures 4 and 5. In Figure 4, we show the angular momentum spectrum at $t = 0$. To verify that the spectrum is well preserved during the simulation, we also plot the spectrum at the time when the apparent horizon is first formed. In Figure 5*a*, we plot $q_* \equiv J(j)/m_*(j)^2$ as a function of $m_*(j)/M_*$. Here $J(j)$ denotes the total angular momentum, with the specific angular momentum j less than a given value j_0, and is defined according

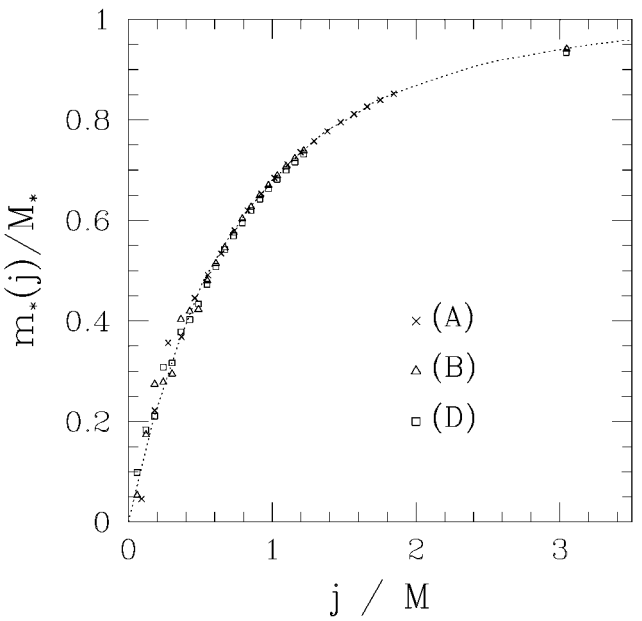

FIG. 4.—Specific angular momentum spectrum at $t \approx 0$ (*dotted curve*) and at the first formation of an apparent horizon at $t \approx 30630M$ for cases D (*squares*), A (*crosses*), and B (*triangles*).

to

$$J(j_0) = \int_{j<j_0} \rho\alpha u^t \psi^6 h u_\varphi \, d^3x. \tag{2}$$

Now $J(j_{\mathrm{ISCO}})/m_*(j_{\mathrm{ISCO}})^2$ and $m_*(j_{\mathrm{ISCO}})$ may be approximately regarded as the instantaneous spin parameter and mass of a black hole, respectively. Therefore, the dotted curve in Figure 5*a*, derivable from the initial stellar profile, may be interpreted as an approximate evolutionary track for the angular momentum pa-

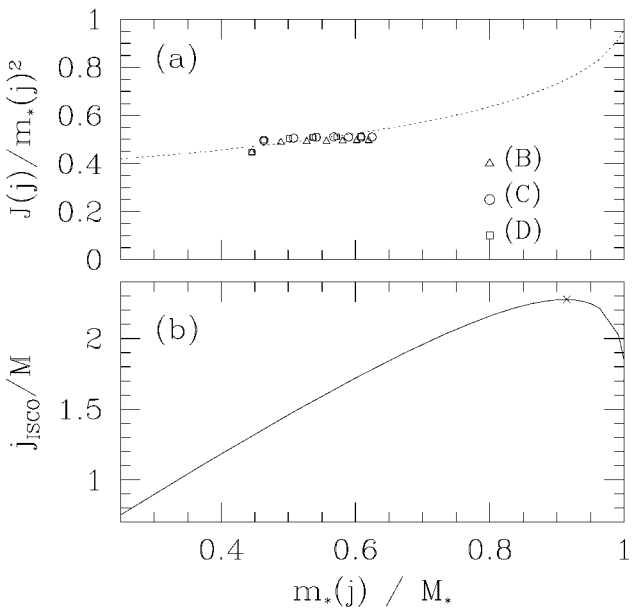

FIG. 5.—(*a*) $J(j)/m_*(j)^2$ as a function of $m_*(j)$ (*dotted curve*). The squares, circles, and triangles show $J_{\mathrm{AH}}/M_{*,\mathrm{AH}}^2$ and $M_{*,\mathrm{AH}}$ at select times for cases D, C, and B, respectively. Here J_{AH} and $M_{*,\mathrm{AH}}$ are the angular momentum and baryon rest mass inside the apparent horizon, respectively. (*b*) j_{ISCO}/M as a function of $m_*(j)/M_*$. The cross marks the maximum.

rameter of the growing black hole. The numerical results for various resolutions indicate that this is close to the actual track followed by the hole. Thus, we can assume that our assumptions made in this analysis are adequate. The dotted curve in Figure 5*a* shows that with the increase of the black hole mass, the spin parameter also increases.

If we assume that $m_*(j)$ and q_* are the mass and spin parameter of the black hole, respectively, and that the spacetime can be approximated instantaneously by a Kerr metric, we can compute $j_{\rm ISCO}$ (see, e.g., Shapiro & Teukolsky 1983). In Figure 5*b*, we show $j_{\rm ISCO}[m_*(j), q_*(j)]$ as a function of $m_*(j)$. For $m_*(j) < 0.9M_*$, $j_{\rm ISCO}$ is an increasing function of the mass. This implies that the mass of the black hole should increase to $\sim 0.9M_*$. However, at $m_*(j)/M_* \approx 0.9$, $j_{\rm ISCO}$ reaches a maximum, as $j_{\rm ISCO}/m_*(j)$ steeply decreases above this mass fraction. Thus, once the black hole reaches this point, it will stop growing dynamically. Figure 5*a* shows that at this stage, $q_* \sim 0.75$. Therefore, at the end of this collapse, (1) about 90% of the total mass will form a SMBH, and (2) the spin parameter of the Kerr hole at the end of the collapse will be ~ 0.75.

4. SUMMARY

We performed a fully relativistic numerical simulation in axisymmetry of the collapse of a uniformly rotating, marginally unstable SMS. Our simulation terminates when roughly 60% of the mass has been swallowed by the SMBH. We estimate that about 90% of the total mass of the system will be consumed by the end of the collapse. The spin parameter q of the final Kerr SMBH is likely to be ~ 0.75 at the end of the dynamical collapse phase. Most of the remaining gas will reside in an ambient disk about the central hole.

To follow black hole growth to a final equilibrium state will require different coordinate gauge choices for the lapse and shift functions. It may also require the use of an "horizon excision" boundary condition (W. Unruh 1984, unpublished; Thornburg 1987; Seidel & Suen 1992). To simultaneously follow the extended disk may necessitate employing a nested grid or adaptive mesh refinement. These issues are ripe for future exploration.

We are grateful to T. Baumgarte, Y. Eriguchi, H. Shinkai, H. Susa, M. Umemura, and K. Uryu for discussion. The numerical computation was performed on FACOM VPP5000 in the data processing center of the National Astronomical Observatory of Japan. This work was supported in part by a Japanese Monbu-Kagaku-sho grant (13740143) and by NSF grant PHY-0090310 and NASA grants NAG5-8418 and NAG5-10781 at the University of Illinois at Urbana-Champaign.

REFERENCES

Alcubierre, M., et al. 2001, Int. J. Mod. Phys. D, 10, 273
Balberg, S., & Shapiro, S. L. 2002, Phys. Rev. Lett., 88, 101301
Baumgarte, T. W., & Shapiro, S. L. 1999, ApJ, 526, 941
Begelman, M. C., & Rees, M. J. 1978, MNRAS, 185, 847
Cook, G. B., & York, J. W. 1990, Phys. Rev. D, 41, 1077
Goldreich, P., & Weber, S. V. 1980, ApJ, 238, 991
Linke, F., Font, J. A., Janka, H.-T., Müller, E., & Papadopoulas, P. 2001, A&A, 376, 568
Loeb, A., & Rasio, F. A. 1994, ApJ, 432, 52
New, K. C. B., & Shapiro, S. L. 2001, ApJ, 548, 439
Quinlan, G. D., & Shapiro, S. L. 1990, ApJ, 356, 483
Rees, M. J. 1984, ARA&A, 22, 471
———. 1998, in Black Holes and Relativistic Stars, ed. R. M. Wald (Chicago: Chicago Univ. Press), 79
———. 2001, in Black Holes in Binaries and Galactic Nuclei, ed. L. Kaper, E. P. J. van den Heurel, & P. A. Woudt (New York: Springer), 351
Saijo, M., Baumgarte, T. W., Shapiro, S. L., & Shibata, M. 2002, ApJ, 569, 349
Schutz, B. F. 2001, preprint (gr-qc/0111095)
Seidel, E., & Suen, W. 1992, Phys. Rev. Lett., 69, 1845
Shapiro, S. L., & Teukolsky, S. A. 1979, ApJ, 234, L177
———. 1983, Black Holes, White Dwarfs, and Neutron Stars (New York: Wi1ey-Interscience), chap. 12
———. 1985, ApJ, 292, L41
Shibata, M. 1999a, Prog. Theor. Phys., 101, 1199
———. 1999b, Phys. Rev. D, 60, 104052
———. 2000, Prog. Theor. Phys., 104, 325
Stark, R. F., & Piran, T. 1987, Comput. Phys. Rep., 5, 221
Thornburg, J. 1987, Classical Quantum Gravity, 4, 1119
Thorne, K. S. 1995, in Proc. Snowmass 95 Summer Study on Particle and Nuclear Astrophysics and Cosmology, ed. E. W. Kolb & R. Peccei (Singapore: World Scientific), 398
Umemura, M. 2001, ApJ, 560, L29
Zel'dovich, Ya. B., & Novikov, I. D. 1971, Relativistic Astrophysics, Vol. 1 (Chicago: Univ. Chicago Press)